Copyright © 2011 by ABCM

STATIC MECHANICAL ANALYSIS OF A SILICON BULK-MICROMACHINED ACCELEROMETER

Janderson Rocha Rodrigues, jrr@ita.br
Aeronautics Institute of Technology, 12228-900, São José dos Campos – SP – Brazil

André da Costa Teves, andreteves@gmail.com
School of Engineering, University of São Paulo, 05508-010, São Paulo – SP – Brazil

Angelo Passaro, angelo@ieav.cta.br
Institute for Advanced Studies, 12228-001, São José dos Campos – SP – Brazil

Luiz Carlos Sandoval Góes, goes@ita.br
Aeronautics Institute of Technology, 12228-900, São José dos Campos – SP – Brazil

Emilio Carlos Nelli Silva, ecnsilva@usp.br
School of Engineering, University of São Paulo, 05508-010, São Paulo – SP – Brazil

Carlos Fernando Rondina Mateus, mateus@ieav.cta.br
Institute for Advanced Studies, 12228-001, São José dos Campos – SP – Brazil

Abstract. *This work describes a static mechanical analysis of a microaccelerometer. This accelerometer is fabricated by bulk micromachining of silicon in KOH solution. The mechanical part of this device consists of an inertial mass suspended by four silicon beams fixed at the edges. The calculation of the equivalent spring constant is done using basic solid mechanics theory. Both large and small deflections cases are analyzed in this study. We determined the Young's modulus and Poisson's ratio according to the crystallographic orientation of the silicon beams. The calculation of the mass and the second moment of area is evaluated taking into account the hexagonal cross section formed during the bulk-micromachined process. The maximum normal stress failure criteria is utilized to determine the maximum stress in the mechanical structure for a given load. The effective mass of the system is calculated discussing the influence of the mass of the beams in the natural frequency and in the static sensitivity of the system. The validity of the model is discussed according to the assumptions and simplifications made. Finally, all analytical results are compared with the ones obtained by the finite element method (FEM). The results show a good agreement between the two methods, validating the analytical model for this kind of analysis.*

Keywords*: MEMS, accelerometer, bulk-micromachining process, static analysis, finite element method*

1. INTRODUCTION

MEMS (Micro-Electro-Mechanical Systems) is a technology that in its most general form can be defined as miniaturized mechanical and electro-mechanical elements i.e., devices and structures, made using the techniques of microfabrication. The micromachined accelerometers are one of the most important types of MEMS devices.

These sensors have broad use in both civilian and military applications, the military ones ranging from missile guidance to inertial navigation systems for aerospace vehicles. In industries, such devices have been widely used in monitoring vibrations of machinery and equipment, as part of routine predictive and preventive maintenance. In automotive industries, accelerometers are used in crash tests as part of the airbags triggering mechanisms, (MNX, 2008).

The micromachined accelerometer can be classified according to the difference of position-sense interface as capacitive, electro-tunneling, magnetic, optical, thermal, piezoelectric as well as piezoresistive. Among all these, capacitive accelerometers have become more attractive and promising for high precision accelerometers due to their simple structure, high sensitivity, good dc response and noise performance, low drift, low temperature sensitivity, low-power dissipation and large readout bandwidth, (Lui *et al*. 2007).

There are two main types of capacitive accelerometer, the surface-micromachined accelerometer, also known as Comb-drive accelerometer, and the bulk-micromachined accelerometer. The surface micromachining builds microstructures by deposition and etching of different structural layers on top of the substrate and bulk micromachining defines structures by selectively etching inside a substrate.

The advantage of the bulk-micromachined accelerometer is the possibility of obtaining large seismic mass, which increases sensitivity, and the large surface area, resulting in large capacitance and easier readout. the disadvantages are the large chip area and the incompatibility of some bulk techniques with CMOS process, (French and Sarro, 1998).

The rise of this technology has stimulated studies about key issues related to solid mechanics and dynamics on the micrometer scale. These issues involve the evaluation of the testing methods for measuring the mechanical properties of MEMS materials, analysis of failure mechanisms of micro-components and analysis of dynamic factors, (Rodrigues *et al*., 2011).

This work describes a static mechanical analysis of a microaccelerometer. This accelerometer is fabricated by bulk micromachining of silicon in KOH solution. The mechanical part of this device consists of an inertial mass suspended by four silicon beams fixed at the edges. The calculation of the equivalent spring constant is done using basic solid mechanics theory. Both large and small deflections cases are analyzed in this study.

We determined the Young's modulus and Poisson's ratio according to the crystallographic orientation of the silicon beams. The calculation of the mass and the second moment of area is done taking into account the hexagonal cross section formed during the bulk-micromachined process. The maximum normal stress failure criteria is utilized to determine the maximum stress in the mechanical structure for a given load. The effective mass of the system is calculated discussing the influence of the mass of beams in the natural frequency of the system.

The validity of the model is discussed according to the assumptions and simplifications made. Finally, all analytical results are compared with the ones obtained by the finite element method (FEM).

2. ACCELEROMETER MODEL

The accelerometer simulated consists of a stack of three bonded silicon wafers, with the hinge springs and seismic mass incorporated in the middle one. The inertial mass forms a moveable inner electrode of a variable differential capacitor circuit. The two outer identical wafers are simply the fixed electrodes of the two capacitors. The differential capacitor senses the relative position of the inertial mass as it displaces under the effect of an externally applied acceleration. Electronic circuit sense changes in capacitance, then convert them into an output voltage.

The air trapped inside the set of wafers acts as a damping system when the seismic mass moves up and down due to an external force acting in the normal direction to the seismic mass surface. In this work, we are mainly concerned with an analytical model to analyse the static behavior of a silicon bulk-micromachined accelerometer. Electric forces and damping due to the internal atmosphere are not taken into account.

The geometric parameters of such device are presented in Table I and Figure 1. The data correspond to the values defined in the accelerometer design, used in the photomask.

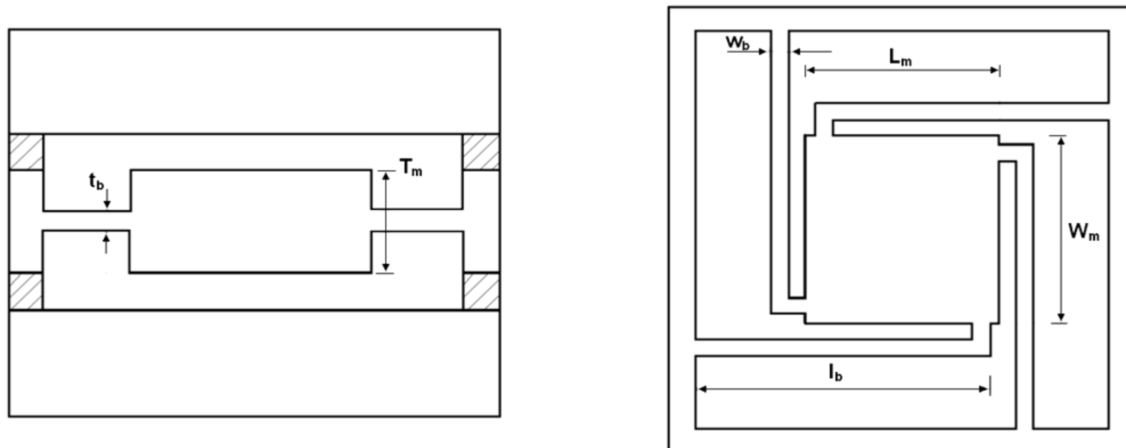

Figure 1. Cross-sectional and planar views of the bulk-micromachined accelerometer

Table 1. Geometric parameters of the accelerometer simulated.

Description	Symbol	Value[μm]
Length of the seismic mass	L_m	2000
Width of the seismic mass	W_m	2000
Thickness of the seismic mass	T_m	380
Length of the beam	l_b	2820
Width of the beam	w_b	177
Thickness of the beam	t_b	55

In summary, the microfabrication of a bulk accelerometer involves a sequence of processes, e.g. thin film deposition, double face litography, simultaneous top and bottom wet etching, bounding of the three wafers.

The wet etching makes use of potassium hydroxide aqueous solution, known as KOH solution. Both sides of the middle wafer are etched, forming the seismic mass suspended by four beams. The KOH solution etchs the monocrystalline silicon anisotropically, i.e., with different etching rate, according to the orientation of the silicon's crystal planes, (Dziuban, 2006). Due to this characteristic, after etching, the geometry of the device has a slightly

different format from de one designed in the mask. The KOH etching process results in beams and seismic mass with an irregular hexagon cross-sectional area, Fig. 2.

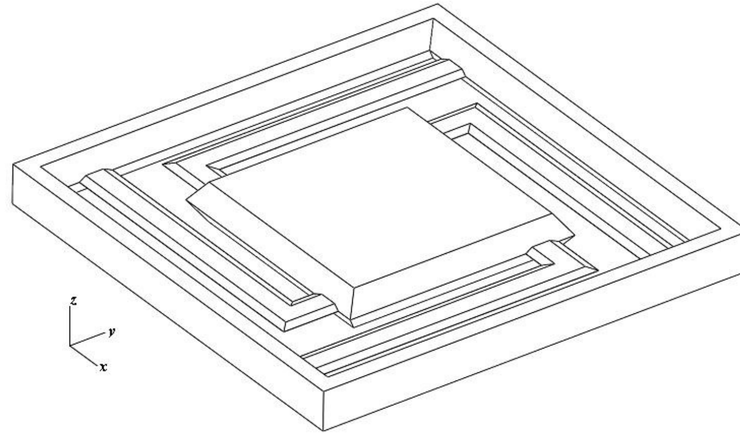

Figure 2. 3D view of middle wafer after KOH etching.

The seismic mass has a form of two truncated pyramids with square base mounted in the opposite way. This format is defined by the (100) plane at the top, and bottom, surrounded by the (111) plane. The angle between the seismic mass' top plane and the seismic mass' edges is 54.74º, (Dziuban, 2006). The thicknesses of seismic mass and the edges are the same as the original thickness of the wafers.

The thickness of the beams is defined during the KOH etching, with the removal of the mask and the formation of high-index planes. The format of the beams is set with (100) plane at the top, and bottom, surrounded by a high-index (411) plane formating an irregular hexagon. The angle between the beam's top plane and the beam's edges is 19.57°, (Dziuban, 2006).

3. ANALYTICAL APPROACH

3.1. Equivalent Spring constant for Small and Large Deflection

The spring constant of the accelerometer can be obtained by using the strength of materials theory. The accelerometer model can be decomposed into two clamped-clamped beam with total length of $2l_b$ and subjected to a concentrated load F_z at the seismic mass. A sketch of a clamped-clamped beam in the z-x plane is represented in Fig. 3:

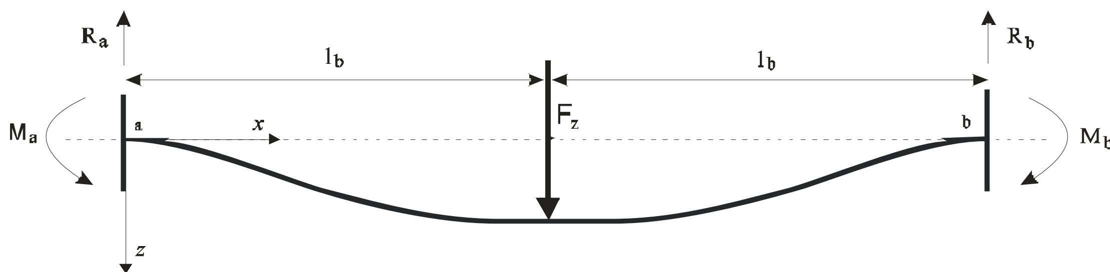

Figure 3. Clamped-clamped beam subjected to a concentrated load.

Due to the symmetry presented in the diagram of Fig. 3, one can deduce that the bending moments at both ends are equal, $M_a=M_b$, the reaction forces at both ends also are equal, $R_a=R_b$, and its absolute value is given by $R_a=R_b=F_z/2$. Taking into account only the rigth hand half of the beam and considering that the beam is composed of a homogeneous material with uniform cross-section, its deflection δ_z can be obtained by the Euler-Bernoulli equation for a concentrated load, (Beer, 2006):

$$EI\frac{d^4\delta_z(x)}{dx^4}=0 \tag{1}$$

where E is the Young's Modulus and I is the second moment of area. Integrating four times Eq. (1) results:

$$EI\delta_z(x) = \frac{C_1x^3}{6} + \frac{C_2x^2}{2} + C_3x + C_4 \tag{2}$$

where C_1, C_2, C_3 and C_4 are the constants of integration and can be found by the boundary conditions, as follows. In the first integral, the shear force is equal to R_a, i. e., $C_1=-F_z/2$. In the Second intregral, taking $x=0$, the bending moment is equal to $-M_a$, i. e., $C_2=M_a$. For the third integral, the slope at the points $x=0$ and $x=l_b$ is equal to zero, $d\delta_z(0)/dx=0$ and $d\delta_z(l_b)/dx=0$, i. e., $C_3=0$ and $M_a=F_z\, l_b/4$. Finally, on Eq. (2) the deflection at point $x=0$ is equal to zero, $\delta_z(0)=0$, i. e., $C_4=0$. Replacing these constant of integraton in the Eq. (2) and Re-arranging terms:

$$\delta_z(x) = \frac{F_z}{24EI}(3l_bx^2 - 2x^3) \tag{3}$$

Eq. (3) has the exact shape of the deflection curve of the beam and is valid between the range ($0 \leq x \leq l_b$). The maximum deflection δ_{zmax} can be obtained taking $\delta_z(l_b)=\delta_{zmax}$, thus:

$$\delta_{zmax} = \frac{F_z{l_b}^3}{24EI} \tag{4}$$

Therefore the spring constant k at z-x plane is obtained directly from Eq. (4). The same procedure is adopted for the clamped-clamped beam in the z-y plane. Taking the spring constant of two parallel clamped-clamped beams result the equivalent spring constant of the accelerometer for small deflections:

$$k_{eq} = \frac{48EI}{{l_b}^3} \tag{5}$$

In the case of large deflections, the analysis has to include the longitudinal axial force N that develops inside the beams. This axial force results in a nonlinear relation between the load F_z and the deflection $\delta_z(x)$. The Euler-Bernoulli's equation with the axial force becomes, (Frish-Fay, 1962):

$$EI\frac{d^4\delta_z(x)}{dx^4} - N\frac{d^2\delta_z(x)}{dx^2} = 0 \tag{6}$$

the detailed solution of the Eq. (7) can be found in Fish-Fay (1962). The center deflection for a concentrated load F_z at the center can be founded by simultaneously solving the next set of equations, (Legtenberg *et al*., 1996):

$$F_z(u) = \frac{EIt_b}{{l_b}^3}\sqrt{\frac{8}{3}}u^3\left(\frac{3}{2} - \frac{1}{2}\tanh^2 u - \frac{3}{2}\frac{\tanh u}{u}\right)^{-\frac{1}{2}} \tag{7}$$

$$\delta_z(u) = t_b\sqrt{\frac{2}{3}}(u - \tanh u)\left(\frac{3}{2} - \frac{1}{2}\tanh^2 u - \frac{3}{2}\frac{\tanh u}{u}\right)^{-\frac{1}{2}} \tag{8}$$

with

$$u = \frac{l_b}{2}\sqrt{\frac{N}{EI}} \tag{9}$$

where u is the common variable and depends on the axial force N, Eq. (9). The equivalent spring constant is obtained doing $F_z/2$ in Eq. (7). Due to this nonlinearity when the deflection increases the spring constant of the beam becomes much larger than in the linear case.

The previous solutions obtained to compute equivalent spring constant for a clamped-clapmed beam in both the small and large deflections, Eq. (5) and Eqs. (7), (8) and (9) are based in a unidimensional model and it assumes that the beams are only subjected to axial stress in one direction, (Mcshane *et al*., 2006). However, the real problem is

intrinsically three-dimensional, thefore when occurs a alongation in the beam in one direction it is accompanied of contraction in another direction. Besides that there is a curvature in the cross section known as *anticlastic effect*, (Kaldor and Noyan, 2005).

These effects are related with the main deflection through Poisson's ratio v. The solution was obtained taking into account that beam's width w_b is small compared to beam's length l_b thefore the stress and its effects in the beam width's direction is negligible. When it is not the case these effects increase the Young's modulus, as described in Eq. (10), (Kampen and Wolffenbuttel, 1998).

$$E_{(w_b/l_b)} = \psi_{(w_b/l_b)} E \tag{10}$$

where $\psi_{(xb/lb)}$ is a adjusment coefficient that is $\psi_{(\infty)}=1$ to a narrow beam and $\psi_{(0)} = 1/(1-v^2)$ to a wide beam. In a wide beam the Young's modulus is called plate modulus. In the next sections, analytical expressions to compute the E, v and I are derived.

3.1.1. Young's Modulus and Poisson' Ratio

Monocrystalline silicion is an anisotropic crystal therefore its mechanical properties vary with respect to cristallographic direction. In a coordinate system coincident with the material cristallographic axes, the most general relationship between the stress tensor, σ_{ij}, and the strain tensor, ε_{kl}, is given by the Hooke's Law, which after some manipulation can be represented in matricial notation as, (Senturia, 2000):

$$\begin{bmatrix} \sigma_x \\ \sigma_y \\ \sigma_z \\ \tau_{yz} \\ \tau_{zx} \\ \tau_{xy} \end{bmatrix} = \begin{bmatrix} C_{11} & C_{12} & C_{13} & C_{14} & C_{15} & C_{16} \\ C_{21} & C_{22} & C_{23} & C_{24} & C_{25} & C_{26} \\ C_{31} & C_{32} & C_{33} & C_{54} & C_{35} & C_{36} \\ C_{41} & C_{42} & C_{43} & C_{64} & C_{45} & C_{46} \\ C_{51} & C_{52} & C_{53} & C_{54} & C_{55} & C_{56} \\ C_{61} & C_{62} & C_{63} & C_{64} & C_{65} & C_{66} \end{bmatrix} \begin{bmatrix} \varepsilon_x \\ \varepsilon_y \\ \varepsilon_z \\ \gamma_{yz} \\ \gamma_{zx} \\ \gamma_{xy} \end{bmatrix} \tag{11}$$

where, τ and γ represents the shear stress and strain, respectively, and the stiffness matrix C_{mn} is symmetric, $C_{mn}=C_{nm}$. Hence, a material without symmetrical elements has 21 independent constants. The stiffness coefficient matrix for cubic-lattice crystals with the vector of stress oriented along the <100> direction is given as, (Senturia, 2000):

$$C_{mn} = \begin{bmatrix} C_{11} & C_{12} & C_{12} & 0 & 0 & 0 \\ C_{12} & C_{11} & C_{12} & 0 & 0 & 0 \\ C_{12} & C_{12} & C_{11} & 0 & 0 & 0 \\ 0 & 0 & 0 & C_{44} & 0 & 0 \\ 0 & 0 & 0 & 0 & C_{44} & 0 \\ 0 & 0 & 0 & 0 & 0 & C_{44} \end{bmatrix} \tag{12}$$

For simplicity, in this work analytical analysis is done in terms of the compliance matrix S_{mn}, where $S_{mn} = C_{mn}^{-1}$. The Young's modulus for an arbitrary crystallographic direction l is given by, Brantley (1973),

$$E_{[l_1,l_2,l_3]} = \left\{S_{11} - 2\left(S_{11} - S_{12} - \frac{1}{2}S_{44}\right)\left({l_1}^2{l_2}^2 + {l_2}^2{l_3}^2 + {l_1}^2{l_3}^2\right)\right\}^{-1} \tag{13}$$

where the l_i are the direction cosines for the vector l. Poisson's ratio is obtained considering a longitudinal stress in the direction l and the transverse longitudinal strain along orthogonal direction p, thus

$$v_{[l_1,l_2,l_3,p_1,p_2,p_3]} = -\frac{S_{12} - \left(S_{11} - S_{12} - \frac{1}{2}S_{44}\right)\left({l_1}^2{p_1}^2 + {l_2}^2{p_2}^2 + {l_3}^2{p_3}^2\right)}{S_{11} - 2\left(S_{11} - S_{12} - \frac{1}{2}S_{44}\right)\left({l_1}^2{l_2}^2 + {l_2}^2{l_3}^2 + {l_1}^2{l_3}^2\right)} \tag{14}$$

where the p_i are the direction cosines for the vector p with repect to the <100> axes. These results are valid for all cubic crystals; for monocrystalline silicon the stiffness elements are C_{11}= 165.7[GPa]; C_{12}=63.9[GPa] and C_{44}=79.7[GPa]. The compliance elements are $S_{11}=7.68\text{x}10^{-12}$[Pa], $S_{12}=-2.14\text{x}10^{-12}$[Pa] and $S_{44}=12.6\text{x}10^{-12}$[Pa], (Wortman and Evans, 1965).

3.1.2. Second Moment of Area

The second moment of area is a proprerty of the beam's cross section. The moment of area of a composite area with respect to a particular axis is the sum of the moments of area of its parts with respect to that same axis, (Gere, 1984). Therefore, in order to compute the second moment of area of the beams with hexagonal cross section, the hexagon was divided in basic components, four triangle and four square, whose the moment of area can be easily obtained. The total moment of area,

$$I = \left(\frac{w_{bm}}{48} + \frac{w_b}{16}\right) {t_b}^3 \tag{15}$$

where w_{bm} is width in the midle of the beam. Taking the angle between the beam's top plane and the beam's edges is possible to find the following relations:

$$w_{bm} = 2\sqrt{2}\, t_b + w_b \tag{16}$$

so we can obtain the second moment of area only in function of the mask design,

$$I = \frac{\left(2\sqrt{2}\, t_b + 4w_{bm}\right){t_b}^3}{48} \tag{17}$$

3.2. Failure Criteria

Silicon behaves as a brittle material at room temperature; in other words, it has no considerable plastic deformation and it is breakable as window glass. However, when the temperature increases to 500-1000°C there is a brittle-to-ductile transition and the silicon behaves as a ductile material, (Hull, 1999). This behavior is also observed in nanometer scale at room temperature as described in Oestlund *et al*. (2009).

Thus, considering the accelerometer is going to work in a temperature below 500°C and is in micrometer scale, silicon is a brittle material; therefore the Maximum Normal Stress Failure Criteria can be adopted. In this criteria the failure occurs when the maximum normal stress σ_{max} reaches the ultimate tensile strength σ_{uts} of the material. The ultimate tensile strength of the monocrystalline silicon is 7000MPa, (Hull, 1999), and the maximum normal stress is given by (Beer, 2006),

$$\sigma_{max} = \frac{M_{max} C}{I} \tag{18}$$

where C is the distance of the neutral surface to the beam's top surface, i. e., $C = t_b/2$, and M_{max} is the maximum bending moment of the clamped-clamped beam, which is given by,

$$M_{max} = \frac{F_z l_b}{4} \tag{19}$$

Substituting C and Eq. (19) into Eq. (18), we have the maximum normal stress for a clamped-clamped beam in function of the applied load.

$$\sigma_{max} = \frac{F_z l_b t_b}{8I} \tag{20}$$

The maximum stress in the whole accelerometer structure is obtained doing $F_z/2$ in Eq. (20). The failure criteria in terms of the safety factor κ is given by,

$$\sigma_{max} < \frac{\sigma_{uts}}{\kappa} = \sigma_{all} \tag{21}$$

where σ_{all} is the maximum normal stress allowable. By defining a security coefficient we can obtain the maximum normal stress allowable and replacing it into Eq. (20) we have the maximum normal force allowable which is proportional the maximum normal acceleration allowable, i.e., shock resistance of the accelerometer.

3.3. Effective Mass

The accelerometer's seismic mass with the geometric form described previously can be obtained by,

$$M_s = \frac{\rho_{Si} T_m}{3} \left({W_{mm}}^2 + W_{mm} W_m + {W_m}^2 \right) \tag{22}$$

where W_{mm} is the width in the middle of the seismic mass and ρ_{Si} is the silicon density that in room temperature is equal to 2330 [kg/m^3], (Hull, 1999). Taking the angle between the seismic mass' top plane and the seismic mass' edges is possible to find the following relations, as in Eq. (16):

$$W_{mm} = W_m + \frac{\sqrt{2}}{2} T_m \tag{23}$$

so we can obtain the seismic mass only in function of the mask design,

$$M_s = \rho_{Si} \left({W_m}^2 \, T_m + \frac{\sqrt{2}}{2} W_m \, {T_m}^2 + \frac{{T_m}^3}{6} \right) \tag{24}$$

The effective mass of beam m_{bef} is obtained using the Rayleigh principle, (Rao, 2003) and (Wai-Chi *et al.*, 2010). This principle uses the relation between kinetic energy of the beam and its deflection curve, for the clamped-clamped beam described in this work it has the form.

$$m_{bef} = \frac{m_b}{2l_b} \int_0^{2l_b} J^2(x) dx \tag{25}$$

where m_b is beam's mass and $J(x)$ is a distribution function given by,

$$J(x) = \frac{\delta_z(x)}{\delta_{zmax}} \tag{26}$$

substituting eqs. (3) and (4) into (26), and solving eq. (25), the effective mass of a clamped-clamped beam is given by,

$$m_{bef} = \frac{13}{35} m_b \tag{27}$$

The effective mass of the accelerometer can then be determined by,

$$M_{eff} = M_s + n \frac{13}{35} m_b \tag{28}$$

where n is the number of beams, in this case n is equal to 2, i. e., there are two clamped-clamped beam.

3.4. Main Parameters

The equivalent spring constant and effective mass can be used to determine two important parameters of the accelerometer the natural frequency f_n given by,

$$f_n = \frac{1}{2\pi} \sqrt{\frac{k_{eq}}{M_{eff}}} \tag{29}$$

Considering the system in static equilibrium,

$$k_{eq}\,\delta_z = M_{eff}\,a_z \tag{30}$$

Thefore, the static sensitivity S_n is given by,

$$S_n = \frac{\partial \delta_z}{\partial a_z} = \frac{M_{eff}}{k_{eq}} \tag{31}$$

where a_z is the acceleration in z direction. For accelerometers, the acceleration is usually given in levels of g, the local standard acceleration of gravity.

The static sensitivity and natural frequency are related by,

$$S_n = \frac{1}{4\pi^2 {f_n}^2} = \frac{1}{{\omega_n}^2} \tag{32}$$

4. RESULTS AND DISCUSSION

The silicon wafer used has orientation (100) and the primary flat is oriented in [110] direction. Accelerometer's beams that are parallel or perpendicular to flat have the same orientation. Young's modulus Eq. (13) and Poisson's ratio Eq. (14) to [110] direction are 168.9 GPa e 0.0642, respectively. The beams in this direction have a very low Poisson’s ratio, taking the worst case, the change in Young's modulus due to lateral effects is only 0.4%, hence, it is negligible.

The Euler-Bernoulli beam equation assumes that the material is homogenous, isotropic, and has the same value of Young’s modulus from compression and tension. Intrisic silicon is a homogenous material, however doped silicon is a heterogenous material and has intrisic stress due to lattice mismatch caused by impurity doping. This intrisic stress is not taken into account in this work. Although silicon is an anisotropic material, it can be shown that the Young’s modulus in a given crystalographic direction, due to compression, is the same as in an opposite direction, due to tension, (Brantley, 1973).

Another assumption is that the material is operating in elastic region. i.e., the material obeys Hooke’s Law. Hence it is valid to monocrystalline silicon and, in this case, it behaves as a brittle material. In both cases, small and large analysis, the slope of the deflection curve is considered small. This assumption is valid in a clamped-clamped beam due to the boundary conditions imposed by the seismic mass and the edges of the accelerometer. It also assumes that there are no residual stress in the accelerometer structure after the micromachining process, which is reasonable for wet etching process.

The normalised deflection as a function of the force is shown in Fig. 4.

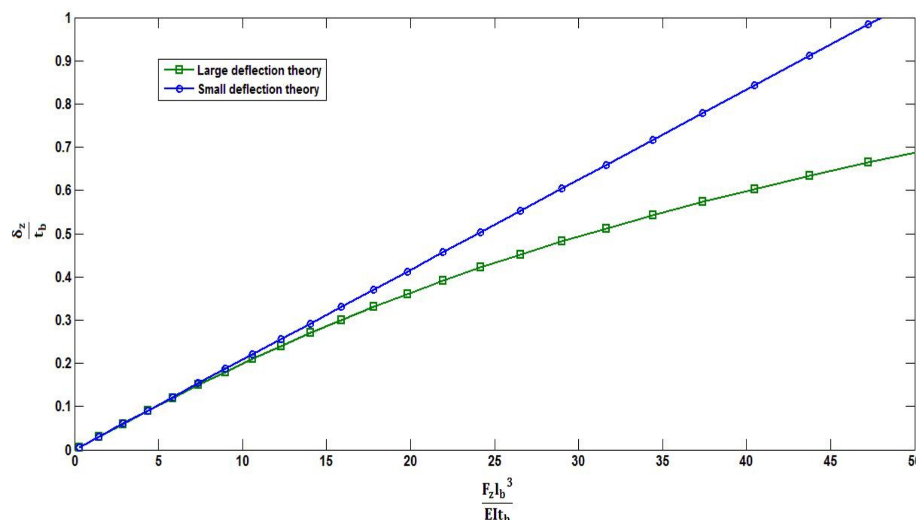

Figure 4. Normalised deflection for small and large theory.

Figure 4 shows that the small deflection theory is valid for deflections up to roughly a quarter of the beam thickness. For deflections above this value large deflection theory has to be used. The beam thickness t_b is 55 [μm] hence the small deflection theory is valid for deflections until 13.75 [μm].

The following figures show the comparison between the results obtained by applying the analytical model in the small deflection theory and a 3D finite elements analysis. The FEM results were obtained using a commercial tool. The 3D model used in the finite element analysis was shown in Fig. 2. The seismic mass deflection versus the applied acceleration is shown in Fig. 5.

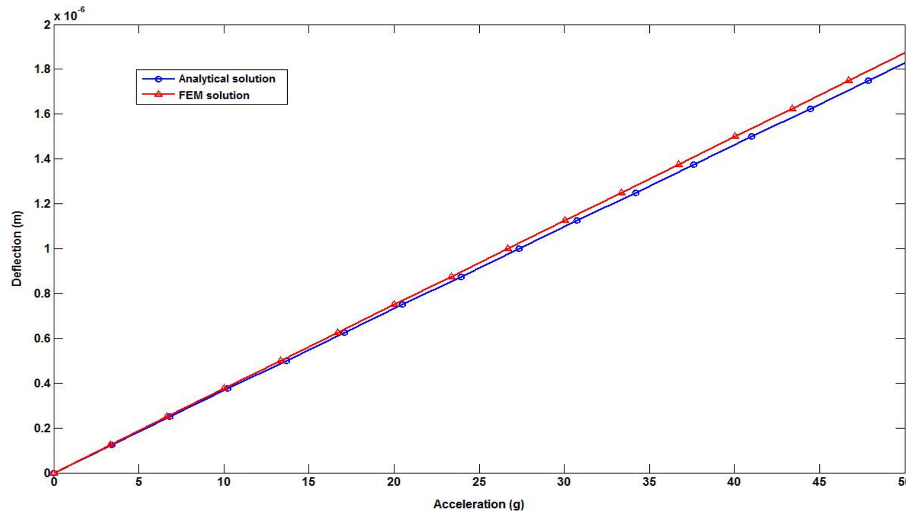

Figure 5. Analytical and FEM results to deflection versus acceleration.

The graph in Fig. 5 shows the seismic mass deflection to applied acceleration, where the static mechanical sensitivity is the slope of the straight lines. The difference between the static sensitivities is of 2.46%.

The model to maximum normal stress, as the bending theory, assumes that the beam is subject to pure bending, i. e., that shear force is zero and no torsional or axial loads are present, therefore there is no stress in x and y directions. The maximum normal stress versus the applied acceleration is shown in Fig. 6.

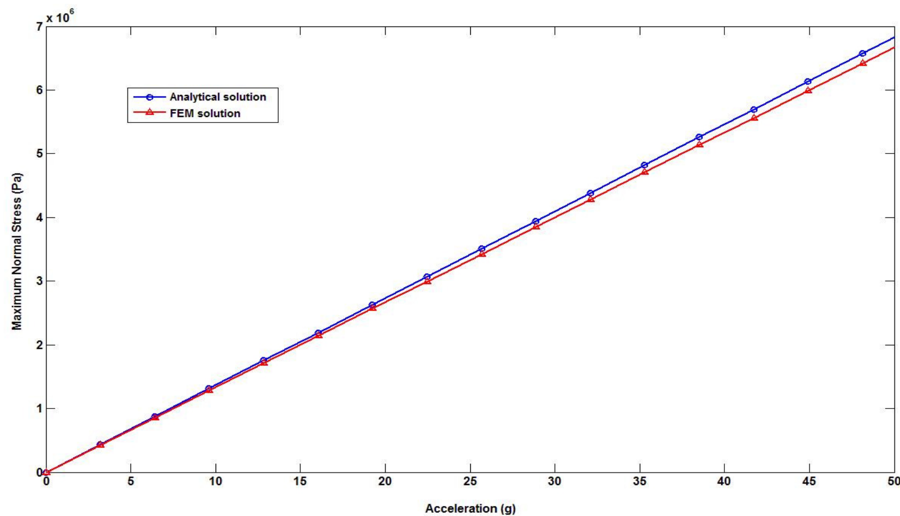

Figure 6. Analytical and FEM results to maximum normal stress versus acceleration.

The results in Fig. 6 show that the analytical model to maximum normal stress described by Eq. (20) is in agreement with the FEM results. The difference between the slopes is 2.46%. The shock resistance of the accelerometer can be determined by the maximum normal stress allowable and therefore the maximum normal acceleration for a given security coefficient.

The natural frequency obtained by Eq. (29) is 2550 [Hz] and the obtained by FEM is 2572[Hz], which results in less than 1.0 percent of error.

Copyright © 2011 by ABCM

5. CONCLUSION

The accurate detemination of mechanical parameters such as natural frequency, shock resistance and static sensibility, are of great techonological importance to characterization and optimization of the accelerometers devices.

The results obtained in this work by applying the analytical model presented for stationary analysis of a bulk-micromachined accelerometer are quite accurate when compared with the FEM results. Moreover, as expected, solving this problem by applying the analytical model is much faster than obtaining the FEM solutions. The analytical analysis can be very accurate depending on the model idealized and the validity of its assumptions. In addition it costs much less in terms of computational resources, which allow its use, for the first phase of computational optimization of such devices, particularly if electrostatic forces and damping due to the internal pressure are taken into account.

6. ACKNOWLEDGEMENTS

This work was supported by FINEP (Brazilian Agency for Funding of Studies and Projects), under grant n: 01.09.0395.00, project ACELERAD. The authors also thanks the financial support of CNPQ (National Council for Research and Development) under grants: 310768/2009-8, 311082/2009-2, and 303689/2009-9.

7. REFERENCES

Beer, F. P., Johnston, E. R. and DeWolf, J. T., 2006, “Mechanics of Materials” Ed. McGraw-Hill, New York, USA, Vol. 4, 400 p.

Brantley, W. A., 1973, “Calculated elastic constants for stress problems associated with semiconductor devices”, Journal of Applied Physics, Vol. 44, pp. 534–535.

Dziuban, J.A., 2006, “Bonding in Microsystem Technology”, Ed. Springer, Netherlands, 331 p.

French, P. J. and Sarro, P. M., 1998, “Surface Versus Bulk Micromachining: The Contest for Suitable Applications”, Journal of Micromechanics and Microengineering, Vol. 8, pp. 45–53.

Frish-Fay, R., 1962, “Flexible bars”, Ed. Butterworths Publications, Washington, USA, 220 p.

Gere, J. M. and Timoshenko, S. P., 1984, “Mechanics of Materials”, Ed. PWS_KENT , Boston, USA, Vol. 2, 400 p.

Hull, R., 1999, “Properties of Crystalline Silicon”, Ed. INSPEC, London, UK, Vol. 20, 1042 p.

Kaldor, S. K., and Noyan, I. C., 2005, “Flexural loading of rectangular Si beams and Plates”, Materials Science and Engineering A, Vol. 399, pp. 64–71.

Kampen, R. P. V. and Wolffenbuttel, R. F., 1998, “Modeling the Mechanical Behavior of Bulk-Micromachined Silicon Accelerometer”, Sensor and Actuators A, Vol. 64, pp. 137–150.

Legtenberg, R., Groeneveld, A. W. and Elwenspoek, M., 1996, “Comb-drive Actuator for Large Displacements”, Journal of Micromechanics and Microengineering, Vol. 6, pp. 320–329.

Lui, X., Zhang, H., Li, G., Chen, W. and Wang, X., 2007, “Design of Readout Circuits Used for Micro-machined Capacitive Accelerometer”, Proceedings of the 2nd IEEE International Conference on Nano/Micro Engineered and Molecular Systems, Bangkok, Thailand, pp. 537–541.

Mcshane, G. J., Boutchich, M., Phani A. S., Moore D. F. and Lu, T. J., 2006, “Young’s Modulus Measurement of thin-Film Materials Using Micro-Cantilevers”, Journal of Micromechanics and Microengineering, Vol. 16, pp. 1926–1934.

MNX, 2008. “MEMS and Nanotechnology Applications” MEMS & Nanotechnology Exchange. 5 Jan. 2011 <http://www.memsnet.org/mems/applications.html>.

Oestlund, F., Rzepiejewska-Malyska, K., Michler, J. et al., 2009, "Brittle-to-Ductile Transition in Uniaxial Compression of Silicon Pillars at Room Temperature", Journal Advanced Functional Materials, Vol. 19, pp. 2439–2444.

Rao, S. S., 2003, “Mechanics of Materials” Ed. Prentice Hall, New York, USA, Vol. 4, 1078 p.

Rodrigues, J. R., Teves, A. C., Passaro, A., Góes, L. C. S., Silva, E. C. N and Mateus, C. F. R., 2011, “Air Damping Analysis of a Differential Capacitive Accelerometer”, Proceedings of the 21st Brazilian Congress of Mechanical Engineering, Natal, Rio Grande do Norte, Brazil, October 24-28

Senturia, S. D., 2000, “Microsystem Design” Ed. Springer, New York, USA, 720 p.

Wai-Chi, W., Azid, A. A. and Majlis, B. Y., 2010, “Formulation of Stiffness Constant and Effective Mass for a Folded Beam”, Journal Archives of Mechanics, Vol. 62, pp. 405–418.

Wortman, J. J., and Evans, R. A., 1965, “Young’s Modulus and Poisson’s Ratio in Silicon and Germanium”, Journal of Applied Physics, Vol. 36, pp. 153–156.

8. RESPONSIBILITY NOTICE

The authors are the only responsible for the printed material included in this paper.